

Experimental and Numerical Investigation of Fluid Flow and Mixing in Pachuca Tanks

E. RODRÍGUEZ M., A.H. CASTILLEJOS E., and F.A. ACOSTA G.

This study reports laboratory and computational work carried out to determine the effect of operating and design parameters on the motion of the liquid and the mixing of a solute in Pachuca tanks. In the laboratory tanks, the liquid velocity field was measured using particle image velocimetry (PIV) and mixing was characterized using a stimulus-response technique. Visualization of the air-water flow suggested the suitability of a one-phase variable density turbulent recirculating flow model coupled to the drift flux model, to describe the motion of the water phase and the gas holdup, in two dimensions (2-D) and in steady state. The dispersion of the solute tracer was simulated by solving the unsteady state turbulent mass transfer equation in three dimensions (3-D). The computational predictions give a good estimate of laboratory measurements of the influence that operating and design variables have on liquid circulation velocity, liquid flow pattern, gas holdup, and mixing evolution and time. Fluid flow simulation of industrial-scale tanks revealed that the recirculating loop that forms in their annular section is more intense and extends over a larger proportion of the reactor height as the draft tube/tank diameters ratio, d_d/d_t , decreases, at the same time the superficial liquid velocity in the draft tube increases. These features suggest that tanks with $d_d/d_t \sim 0.1$ promote conditions for good particle suspension by hindering the settling of particles in the annulus and favoring their lifting in the draft tube; in laboratory-scale tanks, the flow characteristics that enhance particle suspension are not as apparent. The mathematical model also predicts different solute mixing behavior between the laboratory and industrial-scale tanks. At low superficial gas velocities ($u_{sg} \leq 0.003$ m/s) the effect of the increasing d_d/d_t on the decreasing mixing time is smaller in the last tanks. Hence, according to the calculations, it should be expected that industrial tanks with $d_d/d_t = 0.1$ have advantages in regard to particle suspension in comparison to tanks with $d_d/d_t = 0.5$ and, at the same time, they should be comparable in respect to solute mixing under low superficial air velocities, at which they also exhibit good energy efficiency.

DOI: 10.1007/s11663-007-9079-5

© The Minerals, Metals & Materials Society and ASM International 2007

I. INTRODUCTION

PACHUCA tanks are hydrometallurgical reactors in which the suspension of mineral particles and the mass transfer processes controlling the kinetics of the reactions are intimately linked to the motion of the liquid that results from the injection of gas through the base and, in general, into a central draft tube. These tanks are large cylindrical vessels, commonly 4 to 10 m in diameter and 15 m in height, that normally include a tapered base with a 30- to 60-deg half angle and a draft tube typically 0.4 to 1.0 m in diameter.^[1,2,3] These reactor vessels are widely used in the hydrometallurgical industry to carry out gold leaching, uranium leaching, the bacterial oxidation of pyrite, copper leaching, and celestite conversion, among other processes. Their relevance has been claimed to be due to their simple construction, to the absence of moving parts,^[4] and additionally, according to Weiland,^[5] to their low energy

consumption. However, this author^[5] and others^[1,6] indicate that if the ratio of the slurry flow rate to the air flow rate is taken as a measure of the energy performance of the Pachuca tank, this will be high at low gas flow rates, but will become poor after a critical air flow rate is exceeded. In fact, the energy performance will depend on the particular requirements of the process. Fraser^[6] points out that a typical Pachuca tank, operating at an air rate of $0.02 \text{ Nm}^3/\text{min}/\text{m}^3$ of tank volume, may not be able to satisfy the necessary oxygen uptake rate for gold leaching, unless excess air is applied with the consequent waste of energy. For other processes, such as the acid leaching of uranium ores^[4] and celestite conversion,^[7] in which the purpose of the air is the agitation and suspension of particles and not aeration, the process goal may be achieved with a satisfactory energy performance. Lamont^[4] indicated that operations requiring mainly particle suspension and scrubbing are best carried out in full-center column Pachuca tanks, while those needing aeration benefit from the use of free-airlift or stub column tanks. Therefore, based on the needs of a particular leaching process, the operating and design guidelines have to vary.

In the Pachuca tank, the motion of a slurry of mineral particles is established when gas is centrally injected

E. RODRÍGUEZ M., Postdoctoral Student, A.H. CASTILLEJOS E., Professor, and F.A. ACOSTA G., Associate Professor, are with the CINVESTAV–Unidad Saltillo, 25000 COAH, Saltillo, Mexico. Contact e-mail: humberto.castillejos@cinvestav.edu.mx
Manuscript submitted April 4, 2007.

through its base into a draft tube, to produce a liquid upflow within this region and a downflow in the annular space formed between the draft tube and the tank wall. The driving force for this circulation is the imbalance in the hydrostatic heads between these two regions. Clark^[1] and Zaisha *et al.*,^[8] working with Pachuca tanks with a tapered base, found that, at low superficial gas velocities, the flow pattern of the gas phase in the draft tube corresponds to the bubble flow regime. But once the gas velocity increases above a certain limit, the flow regime changes to churn-turbulent or slug. Clark^[1] pointed out that the change in the gas flow regime affects the slurry circulation velocity. Weiland^[5] has indicated that liquid circulation and distribution of the gas phase, as well as the rates of heat, mass, and momentum transfer in Pachuca tanks, are determined by a complex interaction between buoyancy, inertia, friction, and hydrostatic pressure forces; these forces are determined, ultimately, by the operating and design parameters. In his experimental work involving a tank with a flat underside, the author concluded that the ratio of the draft tube to the tank diameters must vary according to the process requirements. He found that d_d/d_t ratios between 0.8 and 0.9 favor mixing and oxygen mass transfer, while a ratio of 0.6 enhances large liquid velocities and good particle suspension. Koide *et al.*^[9,10] reported similar results for this diameters ratio, indicating that the critical gas velocity, defined as the superficial gas velocity required for the complete suspension of solid particles,^[10] has a minimum at a diameters ratio of 0.6. In contrast to these results, Roy *et al.*^[11] found in a laboratory study that the critical air superficial velocity for particle suspension tends to a minimum at $d_d/d_t \sim 0.1$ to 0.2. The authors indicated that this diameters ratio becomes closer to 0.1 (the ratio prevalent in industrial practice) as the tank diameter increases. The critical velocity was found to decrease with the scale-up (increase in diameter) of the tank, *i.e.*, the tanks become more energy efficient as their diameter increases, maintaining a tank height/tank diameter ratio, h_t/d_t , constant. It was suggested that this behavior stems from the increase in the superficial liquid velocity in the draft tube that takes place with the increase in tank diameter, for a given air superficial velocity, u_{sg} , and for given d_d/d_t and h_t/d_t ratios. In another study concerning oxygen mass transfer, Roy and Shekhar^[12] found that the effect of the d_d/d_t ratio (in the range of 0.1 to 0.3) on the oxygen mass transfer coefficient is also affected by the tank scale.

A study on the gas holdup and liquid circulation rate in bubble columns concluded that the overall gas holdup values are smaller and less dependent on the properties of the liquid or liquid-solid phases in columns with a draft tube than in columns without one.^[13] It has been observed that the air holdup increases with an increase in superficial gas velocity,^[13,14,15] but decreases with an increase in the d_d/d_t and h_t/d_t ratios.^[14] Local measurements of gas holdup showed that, in the homogeneous bubble regime, this parameter was uniform over the bubble column cross section, but for other regimes the holdup profiles were symmetrical, with the maximum located at the center.^[13] The mixing of a

solute tracer was studied in laboratory air-lift loop reactors,^[5] and the results showed that the mixing time decreased as the d_d/d_t ratio increased, within the range studied (0.59 to 0.88). Furthermore, the investigator^[5] reported that the mixing time decreases rapidly with the increase in superficial gas velocity, until this reaches a value after which any additional decrease becomes negligible. The scale of the tank also influences the effect that the design and operating variables have on the mixing of solutes. Hence, the effective mixing time, defined as the mixing time per unit reactor volume, decreases with an increase in the reactor volume, and the influence of the d_d/d_t ratio on this parameter becomes also smaller.^[5]

Although many experimental investigations^[1-14] have been carried out about the influence of design and operating variables on fluid dynamics, mass transfer, and particle suspension in Pachuca tanks, less frequent but equally important efforts have gone into predicting these phenomena with the purpose of advancing the design of these reactors. Thus, Lamont^[4] developed a macroscopic energy balance to estimate the liquid circulation flow rate; his analysis established a balance between the energy input by the air, as it expands while rising through the vessel, with that consumed in overcoming the hydraulic heads associated with the air discharge, draft tube friction, and pulp velocity. In a latter work, Clark^[1] calculated an average slurry velocity establishing a macroscopic momentum balance, over the draft tube length, by equating the hydrostatic head over the height of the tank to the sum of the pressure gradients associated with the frictional wall losses, entrance losses, and acceleration losses of the slurry in the draft tube. The author arrived at a design equation that relates the superficial slurry velocity to the superficial air velocity. In a pioneering work, Shekhar and Evans^[16] calculated the single-phase flow motion in the annulus by solving the turbulence Navier–Stokes equation. The two-phase region inside the draft tube was excluded from their analysis by specifying *ad-hoc* boundary conditions at its top and base. The model afforded a qualitative insight into the problem but produced computed flow patterns that were significantly different from those measured in the laboratory.^[3] Singh and Mazumdar^[17] modeled the flow problem by solving the Eulerian motion equation for the liquid, coupled with the Lagrangian motion equation for the gas bubbles and the $k-\epsilon$ model of turbulence. Their predictions regarding the change in the superficial liquid velocity in the draft tube with the superficial gas velocity were reasonable; however, the calculated flow pattern in the annulus did not resemble the experimental one.^[3] On the other hand, the use of a simple algebraic model for estimating the effective viscosity afforded a better representation of the flow pattern in the annulus, but then failed to predict the average circulating velocity in the draft tube. The authors^[17] concluded that the key to a proper mathematical representation of the fluid flow in Pachuca tanks would lie in a more precise modeling of turbulence within the tank annulus. However, previous work^[18] has indicated that the modeling of bubble-driven recirculating flows is more sensitive to

an accurate specification of the spatial distribution of the gas volume fraction.

The literature review shows that mixing,^[5] particle suspension,^[11] and oxygen mass transfer^[12] are affected by design and operating variables to a degree that depends on the size-scale of the Pachuca tank. Hence, there is a need for a mathematical model able to simulate the behaviors observed in the laboratory; that model can then be used to set design and operating criteria for industrial reactors. This article presents both laboratory and computational work on fluid flow and mixing in Pachuca tanks. Apart from encompassing the turbulent mass transfer problem, the main difference of the present mathematical model with respect to previous ones^[16,17] is that the gas volume fraction within the draft tube was evaluated from the simultaneous solution of the turbulent Navier–Stokes equation for a single-phase flow with variable density and the drift flux model^[19] for gas-liquid two-phase flow. The model predicts fairly closely the water velocity fields, the evolution of the solute concentration at the sensor location, and the mixing times for the different experimental conditions investigated. Also, the calculated average gas holdups exhibit good agreement with the results from experimental correlations.^[20] According to the computational results, laboratory and industrial-scale tanks exhibit significant differences in the fluid flow behavior of the liquid, so the laboratory results should be carefully used when trying to understand the functioning of industrial tanks.

II. EXPERIMENTAL WORK

A. Experimental Apparatus and Conditions

A schematic illustration of the experimental setup is shown in Figure 1. The laboratory Pachuca tank was made of Plexiglas and had a conical base at the apex of which a nozzle, 0.002 m in diameter, was placed for the injection of air. For measuring the air flow rate, a rotameter was employed, which maintained the air pressure at 103.4 kPa (15 psig) in all the experiments. A single tank with a diameter of 0.28 m and an underside with a 45-deg half angle was built with sufficient height to allow the selection of the water bath level with respect to the base apex, h_r . Different draft tubes were used to obtain the desired combination of d_d/d_t , h_i/d_t , draft tube submergences, s_d , and draft tube-to-base separations, s_{db} . These design parameters are indicated in the figure.

The Pachuca tank was enclosed in a larger rectangular vessel filled also with distilled water, to minimize parallax effects that would affect negatively the visualization of images. For studying the mixing of a solute, a tilting cup was placed slightly above the bath surface, to pour a tracer solution. The center of the cup was separated from the tank wall by 0.058 m, and aligned with it but 0.35 m below the bath surface a conductivity cell was installed. All this is indicated schematically in Figure 1.

The fluid flow and mixing determinations were done under the operating and design conditions listed in

Table I. From the table, it is seen that a wide range of conditions were covered and that the u_{sg} , d_d/d_t , and h_i/d_t were similar to those of industrial interest cited by Shekhar and Evans.^[3]

B. Experimental Procedures: Fluid Flow Measurements

As seen in Figure 1, the local liquid velocity was measured using a particle image velocimetry (PIV) system based on a diode laser head (Oxford Lasers, HSI 1000, Oxford Lasers Ltd., Didcot, UK), which produces an infrared light sheet (0.05 m high and 0.003 m thick) for illumination of the flow; an electronic unit to control the number, duration, and separation of laser pulses; a charge-coupled device (CCD) camera with a resolution of 1035 (V) \times 1317 (H) pixels (Kodak Megaplug 1.4, Eastman Kodak Co., Rochester, NY, USA); a camera-laser interface; a computer with a frame grabber (Data Translation DT3851, Data Translation Inc., Marlboro, MA); and software for the acquisition and analysis of PIV data (AEA Technology, Visiflow, AEA Technology, Didcot, UK).

For the experimental runs, the water in the tank was seeded with Pliolite (The Goodyear Tire and Rubber Corp., Akron, Ohio) particles (with a density and diameter of 1040 kg/m³ and 63 μ m, respectively) by adding \sim 0.1 kg/m³. Then, the air was turned on to provide the desired u_{sg} and, once steady-state conditions were achieved, the measurement of the local liquid velocity was started. The local velocity vectors were determined from the analysis of double-exposure photographs of tracer particles, which showed them at sequential positions over the plane formed by the thin sheet of laser light. A laboratory-made camera-laser interface was used to synchronize the camera with the laser and generate laser pulse separations from 3 to 20 ms, which were required to detect the low velocities found in the system (\sim 0.01 to 0.4 m/s). The duration of the pulses was 10 μ s. Figures 2(a) and (b) show double-exposure photographs of seed particles passing within the draft tube. When bubbles were present in the field of view, the seed images appeared blurred and the light was scattered by the bubble surface, as seen in Figure 2(a). In contrast, when bubbles were absent (Figure 2(b)), sharp seed image pairs were obtained, from which the local mean water velocities could be determined. This was done using the autocorrelation method implemented in the PIV data analysis software;^[21] in carrying out this analysis, every frame (0.020 (V) \times 0.027 (H) m²) was divided into 21 (V) \times 28 (H) interrogation regions. Thus, the analysis of every frame produced a map of 588 velocity vectors. The validation of the vectors was done by comparing each vector with those close to it; a vector was accepted if its magnitude and direction fell within the bounds defined by visual inspection of the vectors in the respective frame. Spurious vectors were replaced by estimates obtained by interpolation of neighboring ones. The directional ambiguity associated with the autocorrelation analysis of double-exposure images was solved by visual inspection of the flow using a high-speed camera with motion analysis capabilities (Kodak Ektapro, Eastman Kodak Co., Rochester, NY).

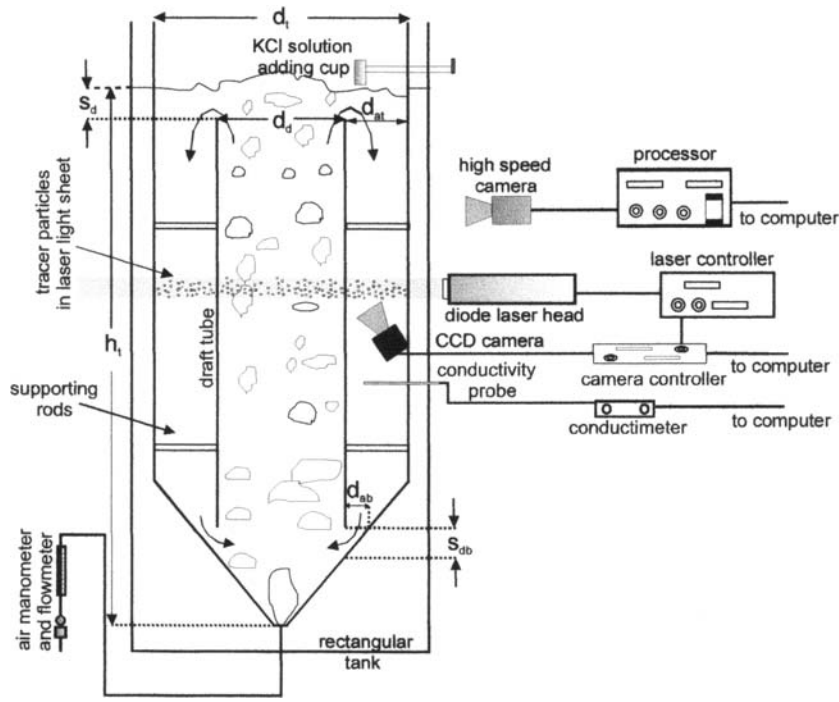


Fig. 1—Schematic diagram of experimental setup.

Table I. Operating and Design Conditions and System Properties Used in the Experimental and Computational Work

$u_{sg} \times 10^3$ m/s	d_d/d_t	h_d/d_t	s_d (m)	s_{db} (m)
Liquid fluid flow field determination				
Experimental 1, 4, 7 Computational 0.125, 0.5, 1, 4, 7	0.25, 0.5	3, 3.14, 3.23, 3.43	0.07, 0.15	0.025, 0.05
Solute mixing evolution and mixing time determination				
Experimental and computational 1, 1.7, 2.4, 3.8, 5, 7	0.1, 0.25, 0.5	2, 3	0.07	0.025
Simulated industrial conditions				
0.125, 0.5, 1, 4, 7	0.1, 0.25, 0.5	2, 3	0.94	2.4
Fluid properties				
ρ_g kg/m ³	1.07			
ρ_l kg/m ³	998			
μ kg/m s	1×10^{-3}			
σ_C	521.65			

C. Experimental Procedures: Mixing Time Measurements

In these experiments, 3 mL of a saturated KCl solution were added after stable fluid flow conditions were established. The change in the electrical conductivity of the bath caused by the addition of the tracer solution was measured by an electrical conductivity probe and recorded in a computer in the form of voltage-vs-time traces. The probe consisted of two stainless steel wires, 0.002 m in diameter and 0.02 m in length, embedded in an epoxic resin and separated by 0.004 m.^[22] The output of the conductivity meter was in the 0- to 1-V range and was proportional to the solute concentration. The current frequencies at which the probe was operated were maintained above 1 kHz, to avoid polarization that would cause wrong measurements.^[23]

The mixing time was defined as the time required to attain a 95 pct level of homogeneity, which was specified in terms of the degree of mixing, Y , as

$$Y = 1 - I_s = 1 - \left| \frac{V_\infty - V(t)}{V_\infty - V_o} \right| \quad [1]$$

where the intensity of segregation, I_s , was expressed in terms of voltage values, because of the proportionality of these values to concentration.

III. MATHEMATICAL MODEL

A. System Considered and Assumptions

Before performing calculations, flow visualizations were carried out during the injection of air in the

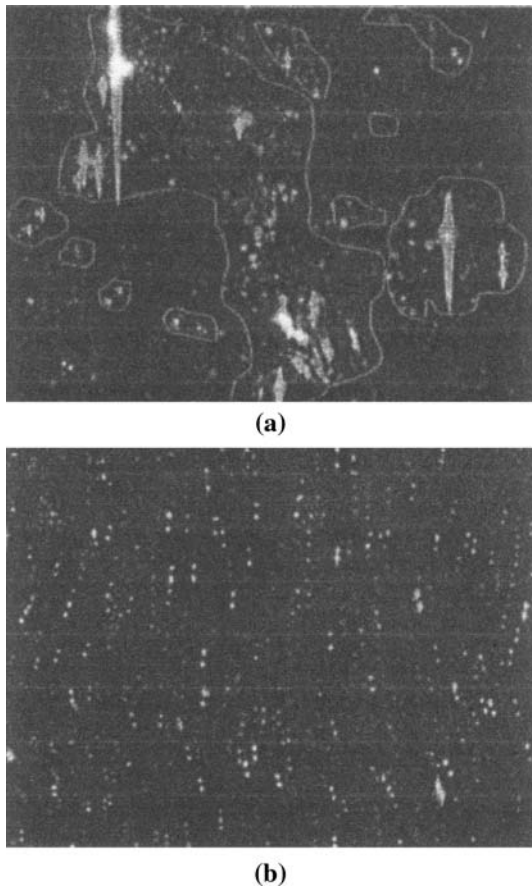


Fig. 2—Double-exposure photographs of seed particles moving through the draft tube at (a) a moment at which bubbles were present in the field of view and (b) a moment at which bubbles were absent from the field of view.

Pachuca tanks, with draft tube diameters of $0.25 d_d$ and $0.5 d_d$, as shown in Figures 3(a) through (d). From the photographs, it can be seen that the air-water flow evolves from the bubbly regime to the churn-turbulent regime as the gas flow rate increases, with the bubbles tending to occupy the whole draft tube diameter as this decreases, *i.e.*, the flow turns to the slug regime. In these systems, the bubbles rise as a column in a fashion very different from the laterally-spreading plumes that are observed in physical models of gas-stirred ladles.^[24] Also, although the gas volume fraction was not measured quantitatively, video films of the rising bubbles suggested that, on a time-averaged basis, there was little variation in the gas volume fraction across the diameter and height of the draft tube; only at the higher flows did the bubbles accumulate above the tube to form a bubble layer with a higher gas holdup. Other features that should be noticed from the photographs are that, except for the highest flows (and, in these cases, only at the top), the annular region was free of bubbles and the free surface remained relatively flat. The physical properties of the system are given in Table I.

Based on these observations, it was assumed that, to establish a fluid flow model, the motion of the water is essentially buoyancy-dominated and the bubble column

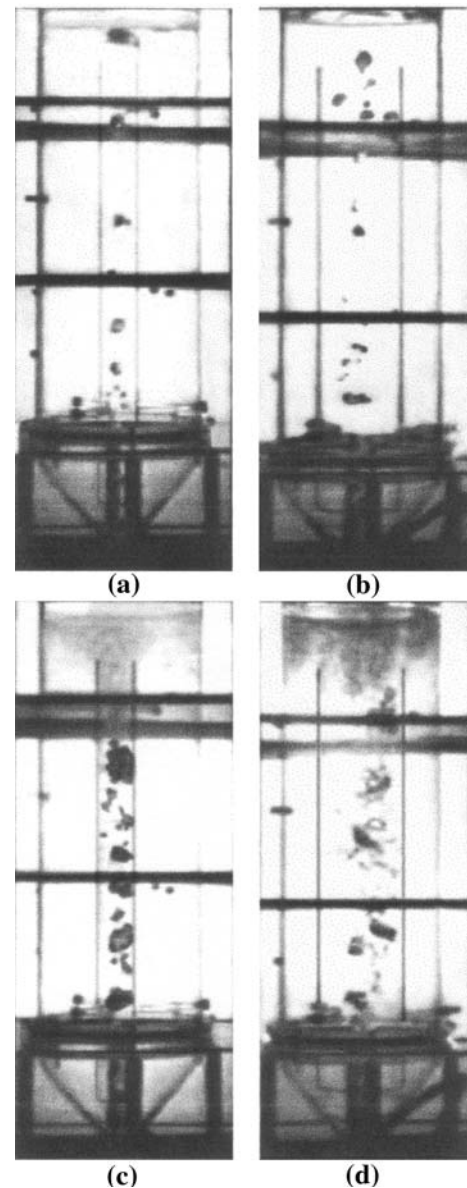


Fig. 3—Photographs illustrating the air-water flow regimes appearing in Pachuca tanks operating under different gas flow rate conditions and with draft tubes of different diameter. Bubbly regime at $Q_g = 0.62 \times 10^{-4} \text{ m}^3/\text{s}$ ($u_{sg} = 1 \times 10^{-3} \text{ m/s}$) for (a) $d_d = 0.07 \text{ m}$ and (b) $d_d = 0.14 \text{ m}$. Churn-turbulent regime at $Q_g = 4.31 \times 10^{-4} \text{ m}^3/\text{s}$ ($u_{sg} = 7 \times 10^{-3} \text{ m/s}$) for (c) $d_d = 0.07 \text{ m}$ and (d) $d_d = 0.14 \text{ m}$.

is axisymmetric and develops in a short time, so that the conditions of two dimensions (2-D) and steady state were considered; the integration domain extended over the axisymmetric plane of the tank. Furthermore, Pachuca tanks have a well-defined boundary between the one-phase and the two-phase region, and the last one has a uniform gas volume fraction distribution across the radial direction, according to the results of Gavroy *et al.*^[13] and the flow visualizations reported earlier. Therefore, it was assumed that the gas holdup in the draft tube varies only in the axial direction according to the drift flux model introduced by Deb Roy *et al.*^[19] for gas-stirred ladle systems, in the form

$$\bar{\alpha} = \frac{1}{2\pi} \frac{Q_g}{\int_0^{r_d} r(u + U_{\text{slip}}) dr} \quad [2]$$

Hence, the flow domain was assumed to be occupied by a single fluid of variable density, ρ , specified as

$$\rho = (1 - \bar{\alpha})\rho_l + \bar{\alpha}\rho_g, \quad \text{for } 0 \leq r < r_d \quad [3]$$

$$\rho = \rho_l, \quad \text{for } r_d + t_w < r < r_t \quad [4]$$

According to the literature,^[1,25,26] the slip velocity, U_{slip} , of bubbles in the slug, churn-turbulent, and bubbly regimes span in the range of 0.18 to 0.45 m/s. In this work, a value of 0.40 m/s was assumed, similar to studies on gas-stirred ladle systems.^[19,27] Also, since the bath-free surface remained relatively quiescent over the majority of the gas flow rates of interest, it was assumed that this was flat and exerted a negligible shear on the air phase above it.

Solute mixing is a time-dependent problem and, in the specific case studied here, was in three dimensions (3-D), due to the position at which the solute was added. Hence, the integration domain was extended to the whole tank described in r - θ - z coordinates. In the circumferential direction, solute mass transfer was supposed to occur only by turbulent diffusion. The effective diffusivity, D_e , was assumed to be the same along the three directions and was evaluated from the solution of the 2-D turbulence fluid flow problem as given in Section III-B. Also, since the solute, KCl, dissolves only in the liquid phase, the whole domain was assumed to be occupied by liquid, so that $\rho = \rho_l$, everywhere. The gas phase was taken into account by blocking the fraction of the discretization cells occupied by it, such that the local liquid volume was given as

$$V_l = V(1 - \bar{\alpha}) \quad [5]$$

B. Governing Equations

Under the assumptions stated here, the governing differential equations for continuity, momentum balance, solute balance, and the turbulence quantities can be written in the general form

$$\frac{\partial \rho \phi}{\partial t} + \nabla \cdot (\rho U \phi) = \nabla \cdot (\Gamma_\phi \nabla \phi) + S_\phi \quad [6]$$

where ϕ stands for the dependent variables given in Table II, together with the expressions for the transport coefficients and source terms. The transient term in the previous expression is zero for all the dependent variables ϕ , with the exception of the solute concentration C . The effective viscosity appearing in the table is given by

$$\mu_{\text{eff}} = \mu + \mu_t \quad [7]$$

Table II. Meaning of Dependent Variables ϕ and Expressions for Γ_ϕ and S_ϕ in the Governing Equations for Turbulent Flow

ϕ	Γ_ϕ	S_ϕ
Continuity equation		
1	0	0
Navier–Stokes equation		
v	μ_{eff}	$-\frac{\partial p}{\partial r} + \frac{\partial}{\partial r} (r\mu_{\text{eff}} \frac{\partial v}{\partial r}) - 2\mu_{\text{eff}} \frac{v}{r^2} + \frac{\partial}{\partial z} (\mu_{\text{eff}} \frac{\partial u}{\partial r})$
u	μ_{eff}	$-\frac{\partial p}{\partial z} + \frac{\partial}{\partial r} (r\mu_{\text{eff}} \frac{\partial u}{\partial r}) + \frac{\partial}{\partial z} (\mu_{\text{eff}} \frac{\partial u}{\partial z}) + \rho_l g \bar{\alpha}$
k - ε turbulence equations		
k	$\mu_{\text{eff}} / \sigma_k$	$G - \rho \varepsilon$
ε	$\mu_{\text{eff}} / \sigma_\varepsilon$	$C_1 \frac{\varepsilon}{k} G - C_2 \rho \frac{\varepsilon^2}{k}$
Solute conservation equation		
C	D_{eff}	0

The turbulent viscosity μ_t was evaluated by the k - ε model^[28] in its conventional form, using the constants^[29] displayed in Table III. Hence, the value of μ_t at any point in the field was calculated from the local values of k and ε according to

$$\mu_t = \frac{C_d \rho k^2}{\varepsilon} \quad [8]$$

The effective transport coefficient of the solute was given as

$$\Gamma_{C,\text{eff}} = \frac{\mu}{\sigma_C} + \frac{\mu_t}{\sigma_{C,t}} \quad [9]$$

where the turbulent Schmidt number for concentration $\sigma_{C,t} \sim 1$.

C. Initial and Boundary Conditions

1. Fluid flow problem

At the axis of symmetry, zero flux conditions were imposed, as

$$v = \frac{\partial u}{\partial r} = \frac{\partial k}{\partial r} = \frac{\partial \varepsilon}{\partial r} = 0 \quad [10]$$

At the bath-free surface, the axial velocities and the stresses were assumed equal to zero, as in

$$\frac{\partial v}{\partial z} = u = \frac{\partial k}{\partial z} = \frac{\partial \varepsilon}{\partial z} = 0 \quad [11]$$

At the walls and base, impermeable and nonslip conditions were imposed, as in

$$v = u = k = \varepsilon = 0 \quad [12]$$

To treat the steep variation in the momentum and scalar transport properties that occur close to solid

Table III. Constants in the k - ε Model

C_1	C_2	C_d	σ_κ	σ_ε
1.44	1.92	0.09	1.0	1.3

walls, the near wall treatment suggested by Launder and Spalding^[29] was applied.

2. Mixing problem

The initial condition established that the tracer was added as a pulse so that, at time $t = 0$, a number of discretization cells with a volume equal to the addition volume (*i.e.*, 3 mL and 76 L for the experimental and industrial-scale cases, respectively) acquired the concentration of the tracer solution; these cells were located just below the addition cup. In the rest of the integration domain, the initial solute concentration was zero. The boundary conditions specified that all the bounding surfaces were impervious to the solute tracer. Furthermore, since the integration domain covered the whole Pachuca tank, cyclic boundary conditions were imposed at two r - z planes, B1 and B2, separated by 360 deg, so that

$$C_{B1} = C_{B2} \quad [13]$$

D. Numerical Procedure

The governing equations for fluid flow and solute mixing were solved uncoupled and in axisymmetrical body-fitted coordinates by the control volume method implemented in the PHOENICS code (CHAM, Ltd., Wimbledon, London, UK).^[30] Depending on the values of the design parameter, the discretized grids for the experimental tanks varied between 56×77 through 56×92 and $56 \times 77 \times 47$ through $56 \times 107 \times 47$ nodes for the flow and mixing problems, respectively; for the industrial tanks, however, the meshes were 168×80 through 100×134 and $168 \times 80 \times 125$ through $100 \times 134 \times 125$. Time steps of 0.5 and 1.0 seconds were used for solving the mixing problem in laboratory and industrial-scale, respectively. These selections ensured grid-independent results in the different problems solved.

The convergence criterion over the domain was set as

$$\sum_{\text{Domain}} |E_{\phi P}| \leq 10^{-3} \quad [14]$$

where $E_{\phi P}$ is the residual of the dependent variable ϕ at position P .

IV. RESULTS AND DISCUSSION

In this section, we present experimental and computational results to discuss the effect of operating and design variables on several parameters characterizing fluid flow and mixing in Pachuca tanks; simultaneously, both types of results are compared. In the case of the velocity field, the evolution of the solute concentration at the measuring point, and the gas holdup, only a selection of results is presented. However, in the case of the liquid circulation velocity and mixing time, the outcomes of all the conditions studied are given. Finally, predictions for industrial-scale tanks are considered.

A. Time-Averaged Velocity Field and Volume-Averaged Gas Holdup

Figures 4(a) and (b) present a comparison between the theoretically-predicted and experimentally-measured velocity fields, for two conditions involving different d_d/d_t ratios and gas superficial velocities. It is seen that the agreement between the measurements and the predictions is good, both in the magnitude of the local velocities and in the flow patterns of the water phase. From the figures, it can be noticed that the recirculating loop that forms on the upper part of the annular region extends over a larger length for tanks with a small d_d/d_t ratio. Additionally, it is observed that the experimental velocity fields display a somewhat disorderly liquid motion in the draft tube that can be attributed to large-scale turbulence fluctuations caused by the pass of bubbles. Moreover, the bubbles during their rise have a swaying motion as a result of interaction with other bubbles, which causes them to deform, break, and coalesce, and thus move the liquid in directions different from the main direction.

A stricter comparison between the experimental and computed velocities is given in Figures 5 and 6, where the axial velocity components are plotted as a function of the radial position for several heights along the tank and for the conditions corresponding to the previous figure. It is seen that, in the annular region, the accord between the predictions and the measurements is excellent. The discrepancies occur mainly in the draft tube at the highest gas superficial velocities; nevertheless, they are relatively small, despite the simple representation of the two-phase region. From the figure, it is also observed that, except for the lower part of the draft tube, the measured and computed profiles of the axial velocity are relatively flat, with the liquid moving in plug flow.

As was mentioned previously, one of the assumptions of the fluid flow model was that the slip velocity of the bubbles was equal to 0.40 m/s, regardless of the air-liquid flow regime prevailing at each particular set of conditions. Therefore, it is appropriate to notice here that the computational experiments showed that halving this velocity increased the predicted liquid velocities in the draft tube by just 10 to 15 pct, *i.e.*, the assumption did not strongly affect the computational results.^[31] To explore further the adequacy of the drift flux model for representing the two-phase region, the predicted volume-averaged gas holdup within the draft tube, defined as

$$\bar{\alpha}_{\text{vol}} = \frac{\int_0^{h_d} \bar{\alpha} dz}{h_d} \quad [15]$$

was compared with the experimental results reported by Shekhar^[15] and with the values calculated from a correlation derived by Hills.^[20] The correlation obtained for bubble columns was rewritten^[15] for Pachuca tanks in the form

$$\bar{\alpha}_{\text{vol}} = \frac{u_{sg,d}}{1.35(u_{sg,d} + u_{sl,d})^{0.93} + 0.24} \quad [16]$$

where the liquid superficial velocity $u_{sl,d}$ was evaluated as the volume average of the predicted u_z velocity component over the draft tube, as

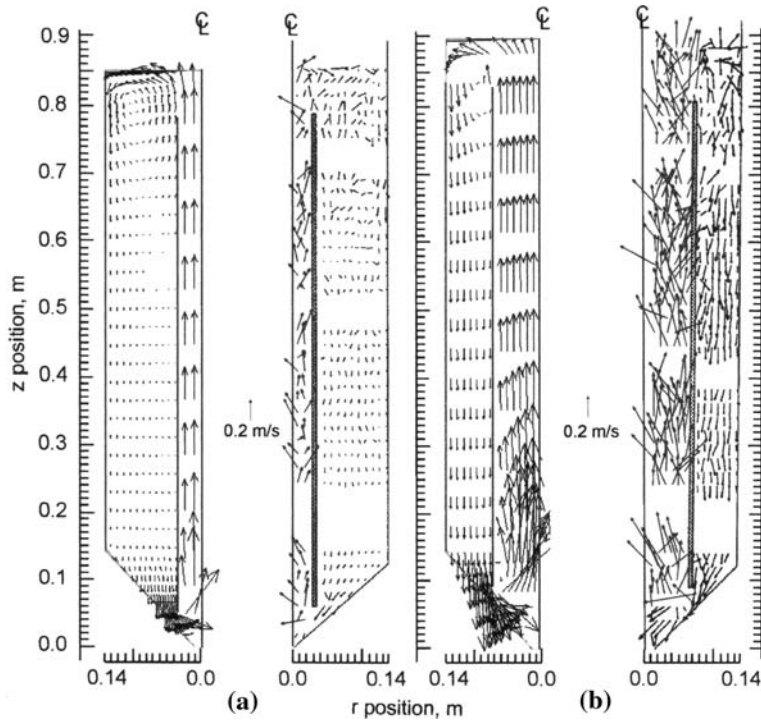


Fig. 4—Predicted and measured mean velocity fields in experimental Pachuca tanks under the following conditions: (a) $u_{sg} = 0.001 \text{ ms}^{-1}$, $d_d/d_t = 0.25$, $h_t/d_t = 3.0$ and (b) $u_{sg} = 0.007 \text{ ms}^{-1}$, $d_d/d_t = 0.5$, $h_t/d_t = 3.14$. The others parameters are $s_d = 0.07 \text{ m}$ and $s_{db} = 0.025 \text{ m}$.

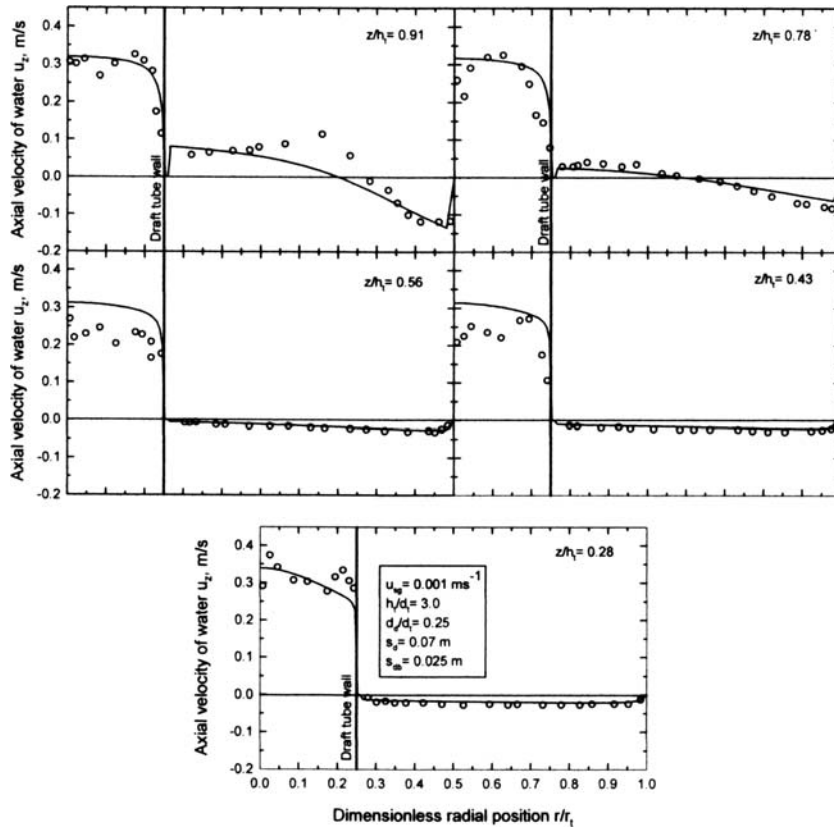


Fig. 5—Comparison between experimental measurements (°) and numerical predictions (-) of the radial variation of the axial velocity component of the water phase, at various axial positions.

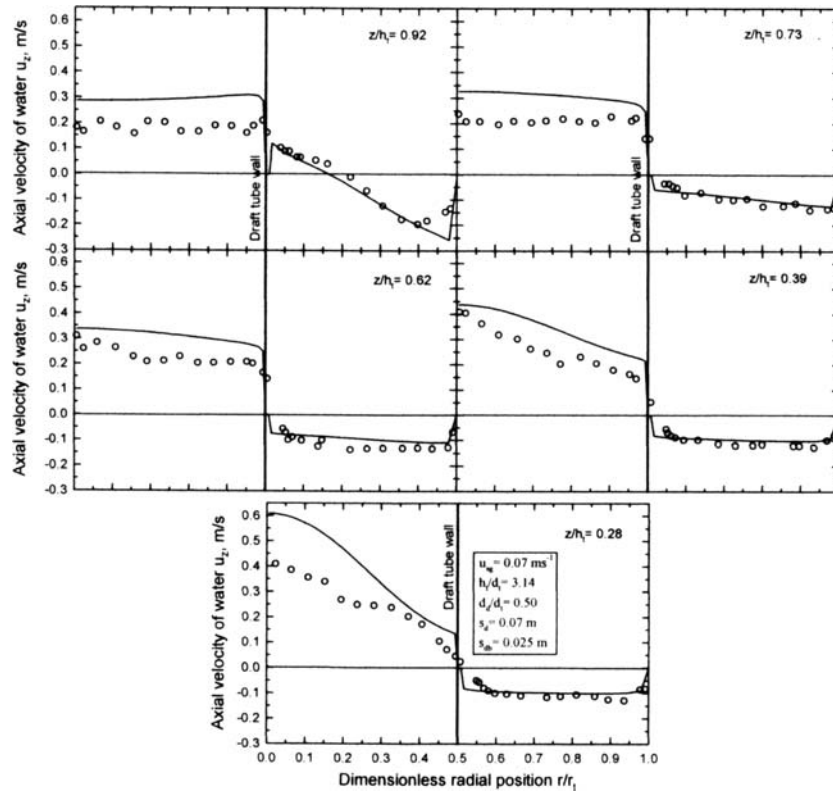


Fig. 6—Comparison between experimental measurements (°) and numerical predictions (-) of the radial variation of the axial velocity component of the water phase, at various axial positions.

$$u_{sl,d} = \frac{\int_0^{r_d} \int_0^{h_d} u_z 2\pi r dr dz}{\int_0^{r_d} \int_0^{h_d} 2\pi r dr dz} \quad [17]$$

The results are shown in Figure 7 for two sets of conditions. From the graph, it is seen that the $\bar{\alpha}_{vol}$ values predicted by the model agree well with those obtained by the correlation, and both show that the gas holdup decreases with the increases in the h_t/d_t ratio, in agreement with the literature.^[14] This behavior stems from the increase in the buoyancy and expansion power of the bubbles as the bath depth increases and causes an increase in the liquid upflow in the draft tube and, hence, a faster travel of the bubbles through the bath. The figure shows that the comparison of the model with the experimental results^[15] is quite good for an $h_t/d_t = 2.1$, but not for a 1.4 ratio. However, in this last case, the measured values did not comply with the trend expected from the effect of the h_t/d_t ratio on the gas volume fraction.

B. Effect of d_d/d_t and h_t/d_t on Water Flow Circulation, Superficial Velocities, and Gas Holdup

Figure 8 shows a plot of the circulating water flow rate, Q_l , as a function of the injected gas flow rate, for two d_d/d_t ratios and several h_t/d_t ratios. The graph includes experimental and predicted values, and it is seen that the agreement between both types of results is

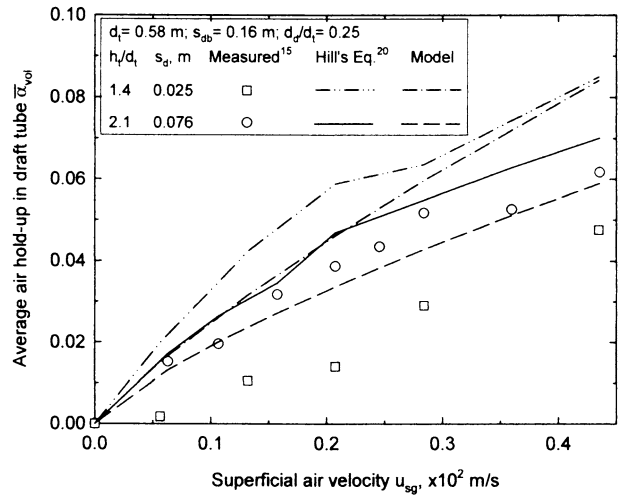


Fig. 7—Plot of the variation of the volume-averaged air holdup in the draft tube as a function of superficial air velocity, comparing experimental, correlation, and model results. The conditions used involved a Pachuca tank with a base cone angle of 45 deg.

excellent. For the range of the parameters h_t/d_t and s_d shown in the figure, it is seen that their effects on liquid circulation are unimportant, but as it is seen later in this article, the influence of h_t/d_t is appreciable when it varies over a wider range. On the other hand, the figure shows that the diameters ratio d_d/d_t has a very significant effect

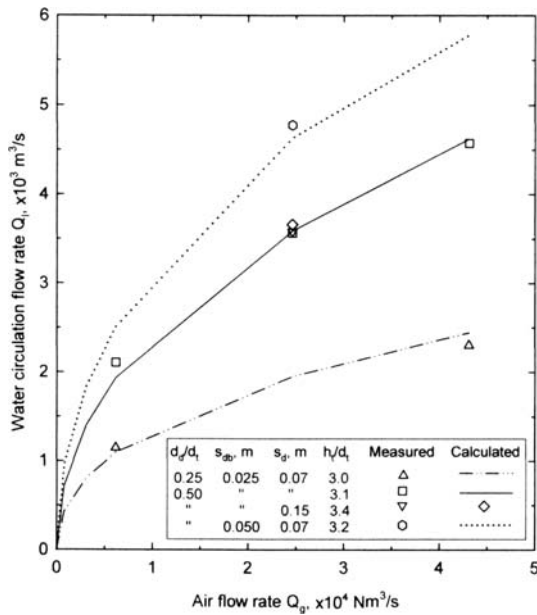


Fig. 8—Circulating water flow rate as a function of air flow rate, for experimental Pachuca tanks with different design parameters.

on water circulation. This result indicates that, with the increase in d_d/d_t ratio, the pressure losses in the draft tube decrease, so that large circulation flows are obtained despite the decrease in the pressure imbalance, $\rho_l g \bar{\alpha}$, responsible for the flow. This argument arises from the calculated variation of the area averaged gas fraction, $\bar{\alpha}$, as a function of the z -position, which is presented in Figure 9 for several d_d/d_t ratios. From the figure, it is seen that the model predicts that $\bar{\alpha}$ decreases with the increase in d_d/d_t , in agreement both with the experimental results of Roy *et al.*^[14] and with the visual observations shown in the photographs of Figure 3. Additionally, it should be noticed from Figure 9 that the gas holdup values predicted by the present model are

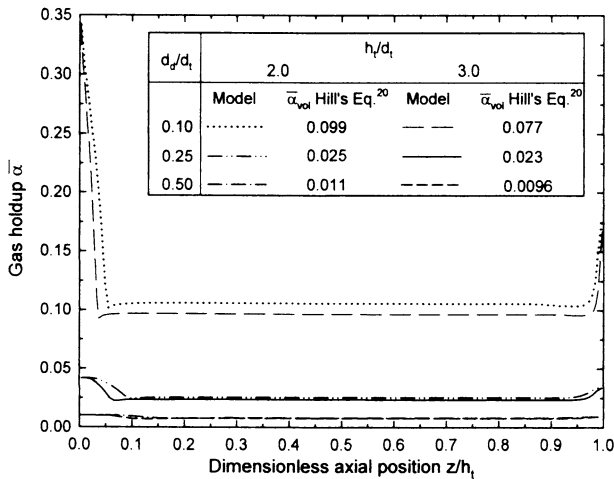


Fig. 9—Variation in gas volume fraction with axial position for Pachuca tanks with different d_d/d_t and h_t/d_t ratios and for $s_d = 0.07$ m, $s_{db} = 0.025$ m, and $Q_g = 0.616 \times 10^{-4} \text{ Nm}^3/\text{s}$ ($u_{sg} = 1 \times 10^{-3}$ m/s).

very close to the $\bar{\alpha}_{vol}$ values calculated from Eq. [16], which are displayed in the key of the figure.

The effect that the distance between the lower end of the draft tube and the base of the tank, s_{db} , has on the water circulating flow was also simulated appropriately by the model, as it can be seen from Figure 8. For the situations modeled, it is observed that the resistance to the flow imposed by the passage formed between the draft tube and the tank base has a significant effect on water circulation. As the water moves from the straight section of the annulus to the tapered one, it converges in the lower end of the draft tube, changing its direction and accelerating. Once the water crosses the passage it diverges and changes its direction drastically, as can be appreciated from the velocity fields presented in Figure 4. Therefore, the model results indicate that the increase in s_{db} tends to moderate the flow changes and reduce the energy losses, resulting in an increased water circulation flow, as can be appreciated from Figure 8. This predicted behavior agrees with the trends of the experimental findings of Koide *et al.*^[9]

The importance of knowing the circulating flow rate of the water in Pachuca tanks is twofold: (1) the circulating flow rate constitutes an index of the rate of transport of the chemical species by bulk flow and (2) it would have a direct influence on the dynamics of the dispersion of the solid particles by determining the superficial water velocities in the annulus, $u_{sl,a}$, and in the draft tube, $u_{sl,d}$. From the mass conservation balance of water, Q_l can be written as

$$Q_l = A_a u_{sl,a} = A_d u_{sl,d} \quad [18]$$

Large $u_{sl,d}$ values would produce a large upward drag of the particles in the draft tube, while a low $u_{sl,a}$ would cause a small downward drag of the particles in the annular region; this combination of factors would promote lifting and a reduced sedimentation of the particles in the draft tube and annular section, respectively. Hence, from Figure 10, which shows the variation in $u_{sl,a}$ and $u_{sl,d}$ with the superficial air velocity, it may be expected that small d_d/d_t (~ 0.1) ratios would favor better particle suspension than would large ones. Furthermore, the figure shows that the absolute values of the superficial velocities and, as a consequence, the water circulation flow rate increase with the h_t/d_t , for a given superficial air velocity. A qualitative insight about the effect that an increment in this parameter would have on particle dispersion is difficult to assess from the information provided by the figure, since this suggests that it would simultaneously enhance particle lifting in the draft tube and sedimentation in the annulus. However, this and other aspects of particle dispersion are currently under investigation.^[31]

C. Effects of u_{sg} , d_d/d_t , and h_t/d_t on Solute Mixing and Flow Turbulence

From the results just presented, it should be noticed that the numerical solution of the turbulent Navier–Stokes equation provides a great deal of information on

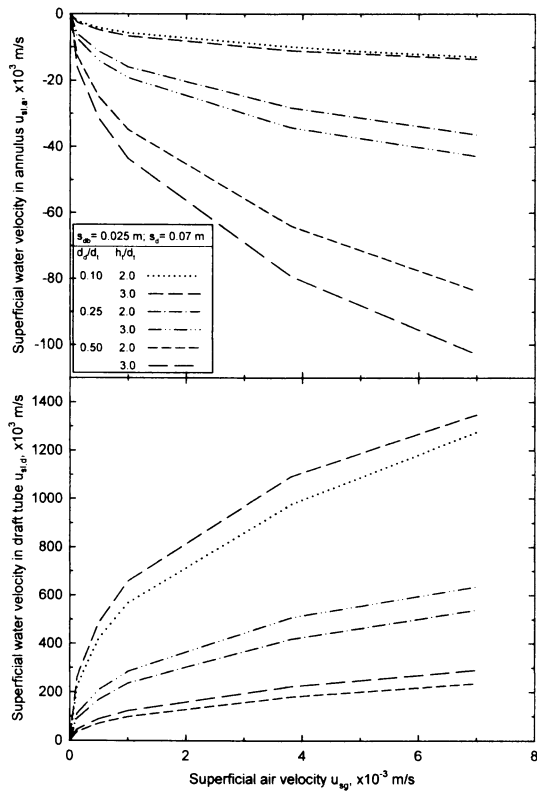


Fig. 10—Predicted superficial water velocities vs superficial air velocity, comparing the effects of different d_d/d_i and h_i/d_i ratios.

the velocity fields and the gas holdup distribution, and suggests how the bulk liquid motion may affect solute mixing and particle suspension. On the other hand, this section discloses how the solution of the solute mass conservation equation complements that information by distinguishing the contributions of the bulk liquid motion and the turbulence on solute mixing and by pointing out the effect that the operating and design parameters have on it.

Figures 11(a) and (b) show comparisons between experimentally-measured and theoretically-predicted tracer dispersion curves for laboratory Pachuca tanks with h_i/d_i ratios equal to 2 and 3, respectively. It may be seen that, while the mathematical model does not exactly match the measured curve, it does predict the overall trend quite well; in many cases, it is quite accurate in predicting the time required for the complete homogenization of the aqueous solution, as shown in Figures 12(a) and (b). In these figures, it is seen that, with the increase in superficial air velocity, the mixing improves rapidly until the velocity is about 3.8×10^{-3} m/s, while at higher velocities, mixing becomes less efficient.

Comparing Figures 12(a) and (b), it is appreciated that the mixing time increases with increases in the tank size, *i.e.*, h_i/d_i , despite the superficial liquid velocities augments (*i.e.*, the water circulation flow rate) with the increase in this ratio, as reported in Figures 10(a) and (b). The turbulence energy fields shown in Figure 13 suggest that this behavior arises because the zone with low turbulence levels (found in the lower part of

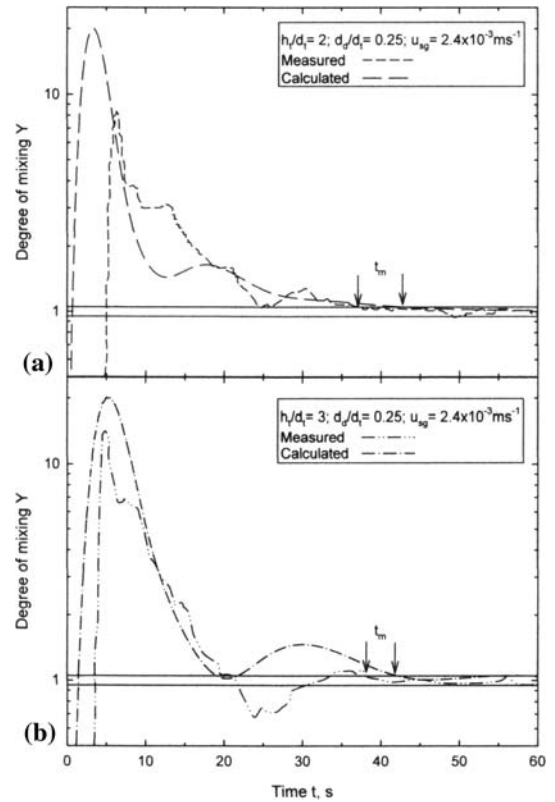


Fig. 11—Evolution of solute tracer dispersion at the conductivity sensor position for Pachuca tanks with (a) $h_i/d_i = 2$ and (b) $h_i/d_i = 3$; other conditions are the same.

annulus) occupies a greater proportion of the tank as h_i/d_i increases, for a given u_{sg} and d_d/d_i ratio. Hence, as expected, turbulence plays a very important role in the complete mixing of solutes.

Additionally, the measured and predicted results given in Figures 12(a) and (b) show that, for a given superficial air velocity, the influence of the diameters ratio d_d/d_i on the time of mixing decreases with the tank size, *i.e.*, the mixing time decreases as the d_d/d_i increases in tanks with $h_i/d_i = 2$, while it is almost the same for diameters ratios equal to 0.25 and 0.5 in tanks with $h_i/d_i = 3$. Apparently, the reason for this behavior is, again, the variation in the turbulence level and the turbulence pattern with the tank configuration. As the plots of Figure 13 show for the smaller d_d/d_i ratio, the turbulence level at the base of the draft tube is larger and the regions of higher turbulence at the top of the annulus are more extensive compared to those for the bigger ratio; additionally, these changes are more acute for the larger h_i/d_i ratio. This behavior indicates that the relative importance of water circulation velocity and turbulence on mixing time is a function of tank size and geometry.

D. The Predicted Behavior of Industrial-Scale Tanks

Since the previous sections show that the fluid flow and mass transfer models give a good account of the behaviors observed in the experiments, this section

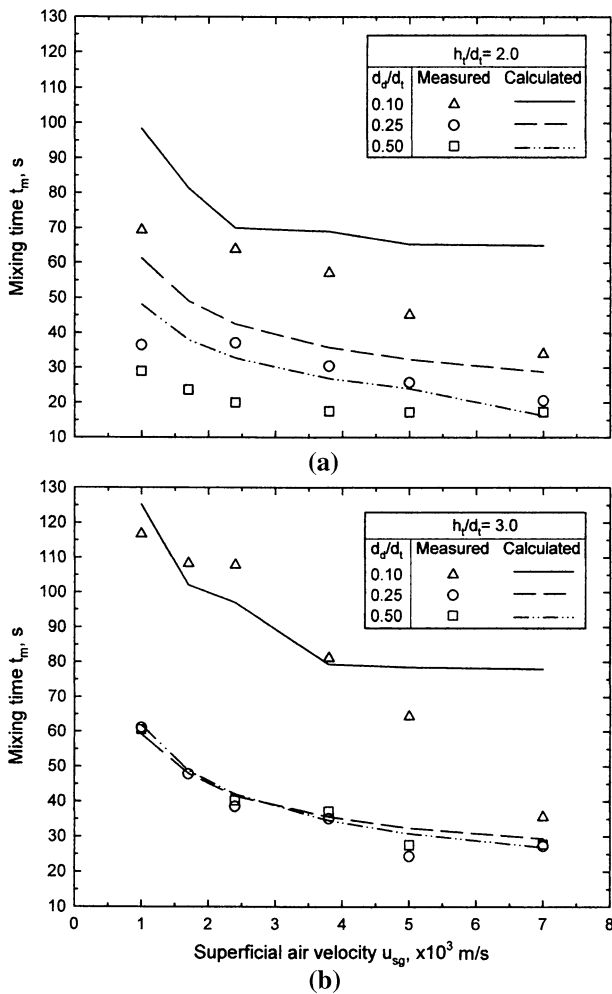


Fig. 12—Measured and predicted mixing time as a function of superficial air velocity for laboratory Pachuca tanks with different diameters ratios and for (a) $h_i/d_t = 2$ and (b) $h_i/d_t = 3$.

presents the predictions for industrial-scale Pachuca tanks, the ultimate goal of this work.

The calculations for the industrial-scale tanks have been done for three superficial air velocities and for a particular set of tank dimensions that is within the range used in the industry. The computations involved two diameters ratios; for comparison with laboratory-scale tanks, the areas ratios A_{ct}/A_a and A_{cb}/A_a in both scales were the same, so that energy losses due to the flow reversal at the upper and lower ends of the draft tube should be expected to be similar.

Figures 14 and 15 show the velocity fields computed for the experimental and industrial-scale tanks for d_d/d_t equal to 0.1 and 0.5, respectively. For the small diameters ratio (Figure 14), it is seen that the calculated fraction of the tank height occupied by the recirculating loop formed in the annulus is much larger for the industrial-scale tank than for the equivalent laboratory-scale tank. The large velocities at which the liquid exit the draft tube cause strong currents to hit the tank wall, which then move backward against the draft tube to recirculate. From the large recirculating loop formed in

the industrial-scale tank, it should be expected that, if particles were present, a large proportion of them would be maintained in suspension, while those moving to the base of the tank through the annulus would be lifted by the large ascending velocities once they reach the entrance of the draft tube. For $d_d/d_t = 0.5$, the predicted flow patterns for tanks of both scales are very similar, with the height fraction of the recirculating loop being relatively short, as can be appreciated from Figure 15. In this case, it could be thought that, if particles were present, a large proportion of them would move mainly downward, settling on the tank underside and possibly hindering the entrance into the draft, where they would be picked up by the ascending water currents. Therefore, it should be expected that a $d_d/d_t = 0.1$ would be more suitable for particle suspension than would be a larger ratio.

Figure 16 shows the ratio of the superficial liquid velocity in the annulus to the superficial gas velocity, as a function of the latter. From the figure, it is seen that the model predicts that, in industrial-scale tanks, the water circulation velocity that can be achieved at a given superficial air velocity is larger than that obtained in the laboratory-scale tanks. The predictions show that the efficiency of the industrial tanks with respect to their equivalent laboratory tanks is larger for $d_d/d_t = 0.1$ than it is for tanks with $d_d/d_t = 0.5$, at low superficial air velocities (≤ 0.004 m/s), while the opposite is true for larger velocities. Thus, the model indicates that the effect of the design parameters on the fluid flow depends on the operating conditions and the size scale. Therefore, the laboratory work should be used cautiously in trying to interpret the behavior of industrial tanks.

The variation in the mixing time with the superficial air velocity for different d_d/d_t ratios is shown in Figure 17 for an industrial-scale tank. Again, the behavior predicted for large-sized reactors is different from those of laboratory-scale reactors; this was displayed in the plots appearing in Figure 12. In large-scale reactors and in the range of $0.001 \leq u_{sg} \leq 0.004$ m/s, the effect of the d_d/d_t increases with the increase in the superficial air velocity, starting from being nil at $u_{sg} = 0.001$ m/s. From these results, it should be expected that, at low superficial gas velocities ($u_{sg} \leq 0.003$ m/s), a tank with a $d_d/d_t = 0.1$ should present advantages in regard to particle suspension and energy efficiency in comparison to a tank with $d_d/d_t = 0.5$, and at the same time, should be competitive with respect to solute mixing. Although according to Figure 16, industrial-scale tanks with a $d_d/d_t = 0.5$ involve larger water circulation velocities and, hence, should be more effective for solute transport by bulk motion, they are not as effective for providing complete mixing, because of their smaller turbulence levels, as is seen by comparing Figure 18(b) with Figure 18(a). From Figure 18(a), corresponding to $d_d/d_t = 0.1$, it may be expected that the large turbulence levels present at the base of the draft tube and at the top of the bath should contribute to homogenize the solute in the bath, particularly by favoring its transport along the circumferential direction by turbulent diffusion.

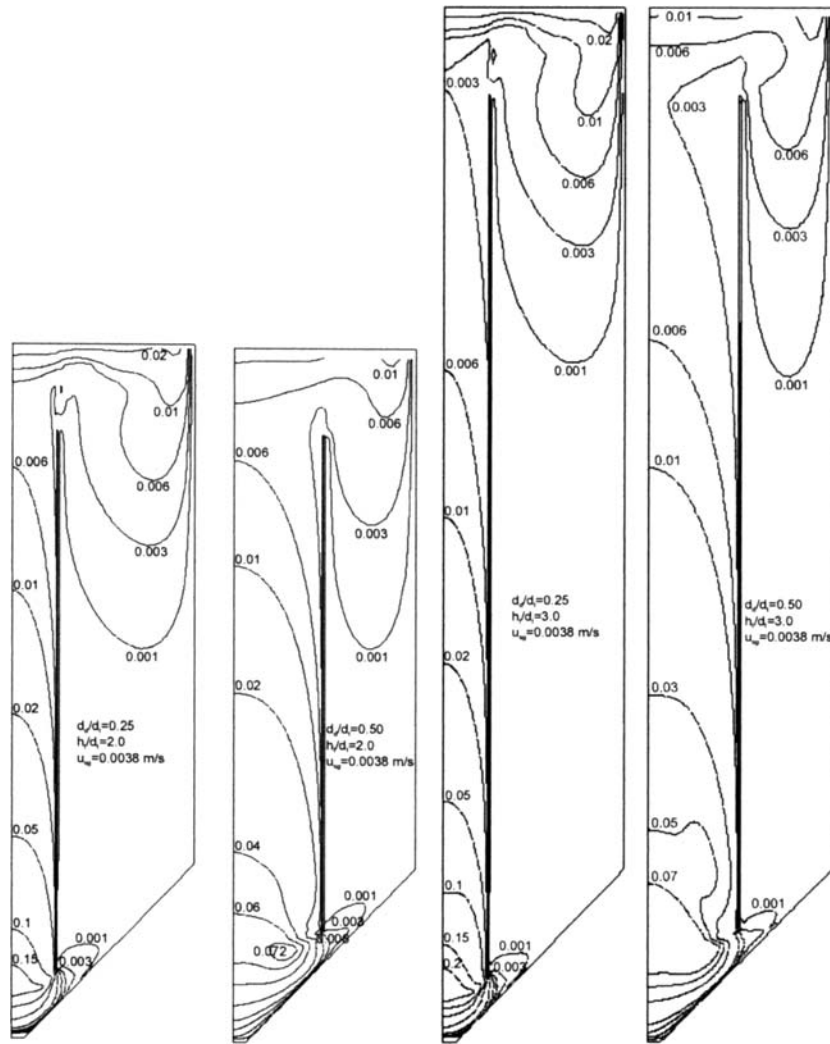


Fig. 13—Predicted distributions of turbulent kinetic energy in laboratory Pachuca tanks with two different h_t/d_t and d_d/d_t ratios and a single superficial air velocity.

V. SUMMARY AND CONCLUSIONS

This article reports laboratory and computational work carried out to determine the effect of operating and design parameters on the motion of the liquid and the mixing of a solute in Pachuca tanks. The turbulent recirculating flow model, which uses the drift flux model to represent the two-phase air-water region, gives a good representation of the laboratory measurements in regard to the influence that operating (u_{sg}) and design (d_d/d_t , h_t/d_t , s_d , and s_{db}) variables have on the liquid circulation velocity, liquid flow pattern, gas holdup, and mixing evolution and time. The good representation of the experimental results regarding solute mixing seems to substantiate the validity of the predicted turbulence quantities k and ϵ .

The use of the model to simulate the behavior of industrial-scale tanks revealed that the recirculating loop that forms in the annular section of the tanks is more intense and extends over a larger proportion of

the reactor height as the draft tube/tank diameters ratio, d_d/d_t , decreases, at the same time the superficial liquid velocity in the draft tube increases. From the large recirculating loop formed in industrial-scale tanks with $d_d/d_t = 0.1$, it should be expected that, if particles were present, a large proportion of them would be maintained in suspension, while those moving to the base of the tank through the annulus would be lifted very energetically by the strong ascending water current, once reaching the entrance of the draft tube. Moreover, the efficiency of industrial-scale tanks in generating bulk water motion (*i.e.*, $u_{sl,a}/u_{sg}$) is greater than that of laboratory-scale ones. At low superficial air velocities ($0.001 \leq u_{sg} \leq 0.004$ m/s), the proportion in which their efficiency augments relative to laboratory-scale tanks is larger for $d_d/d_t = 0.1$ than for $d_d/d_t = 0.5$. Also, the model indicates that, in industrial tanks at low u_{sg} values (0.001 to 0.003 m/s), the increase in mixing time with the decrease in the d_d/d_t is relatively minor.

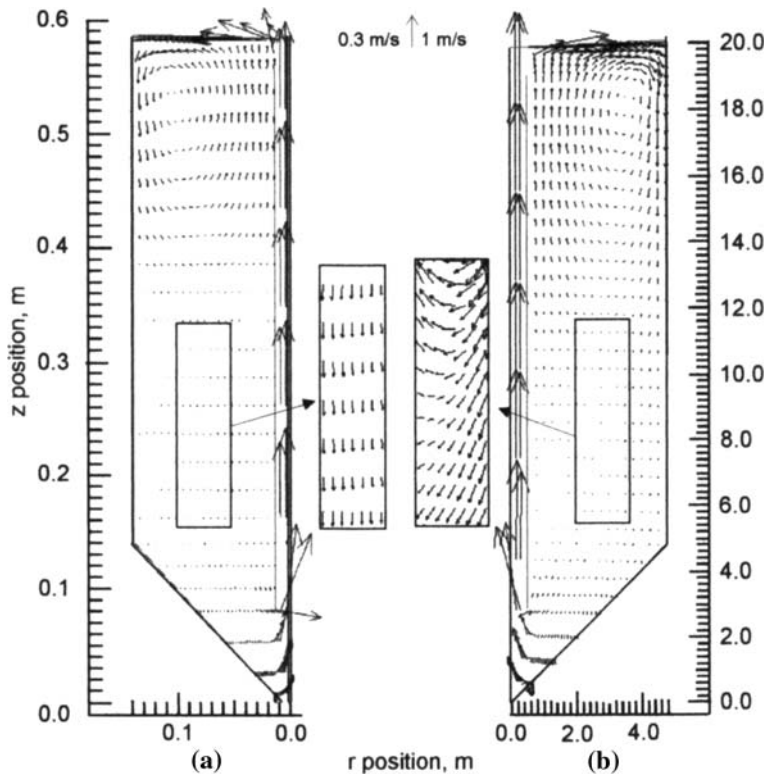


Fig. 14—Predicted mean velocity fields for (a) experimental tank with $d_t = 0.28$ m, $s_d = 0.027$ m, and $s_{db} = 0.076$ m and (b) industrial tank with $d_t = 9.60$ m, $s_d = 0.94$ m, and $s_{db} = 2.39$ m. The other conditions are: $u_{sg} = 0.001$ m/s, $h_t/d_t = 2.08$, $A_{cl}/A_a = 0.040$, $A_{cb}/A_a = 0.304$ and $d_d/d_t = 0.1$.

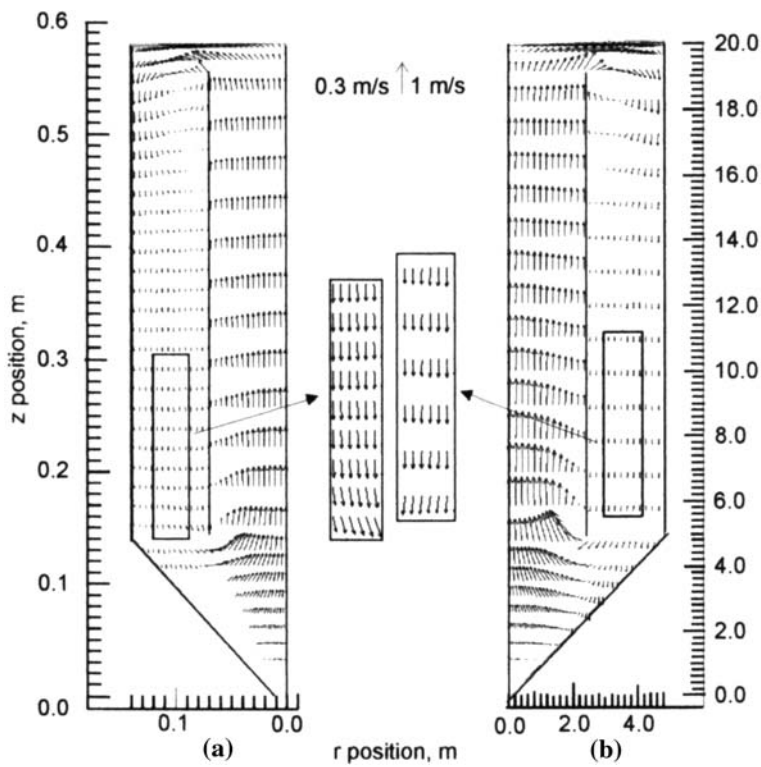


Fig. 15—Predicted mean velocity fields for (a) experimental tank with $d_t = 0.28$ m, $s_d = 0.027$ m, and $s_{db} = 0.076$ m and (b) industrial tank with $d_t = 9.60$ m, $s_d = 0.94$ m, and $s_{db} = 2.39$ m. The other conditions are: $u_{sg} = 0.001$ m/s, $h_t/d_t = 2.08$, $A_{cl}/A_a = 0.261$, $A_{cb}/A_a = 0.70$, and $d_d/d_t = 0.5$.

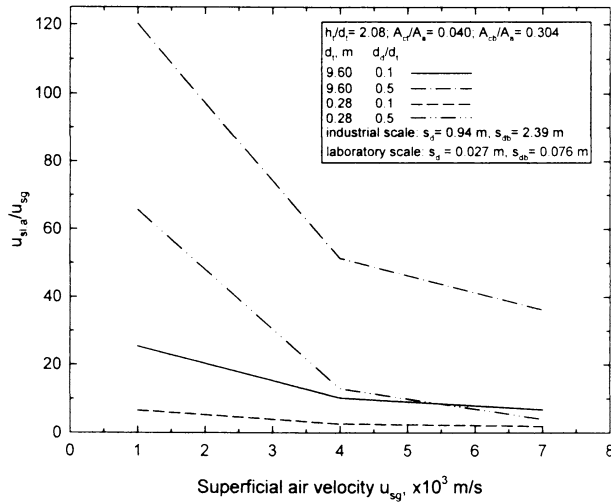


Fig. 16—Plot of the proportion of the superficial water velocity in the annulus with respect to the superficial air velocity as a function of the latter, for laboratory and industrial-scale tanks.

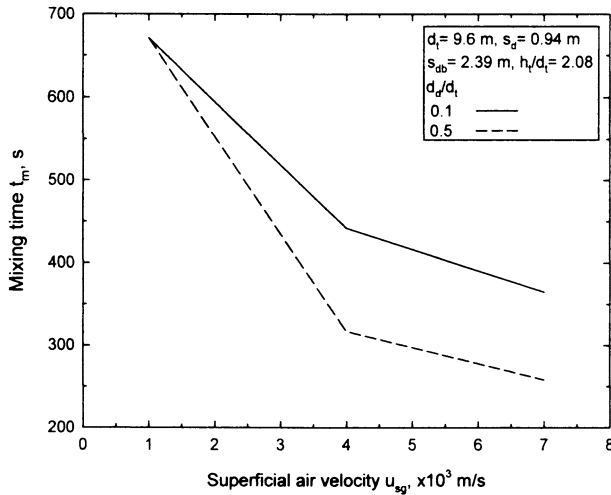


Fig. 17—Predicted mixing time as a function of superficial air velocity for industrial Pachuca tanks with different diameters ratios.

Hence, according to our computer model, it should be expected that industrial tanks with $d_d/d_t = 0.1$ would have advantages in regard to particle suspension in comparison to tanks with $d_d/d_t = 0.5$ and that, at the same time, they should be comparable in respect to solute mixing under appropriate operating conditions, at which they are also energy efficient. Finally, since the flow characteristics that are responsible for the predicted behavior of industrial tanks (with $d_d/d_t = 0.1$) are not as noticeable in laboratory-scale tanks, it was very important to arrive at a mathematical model that allows quantitative predictions and that can be extended to the study of particle suspension.

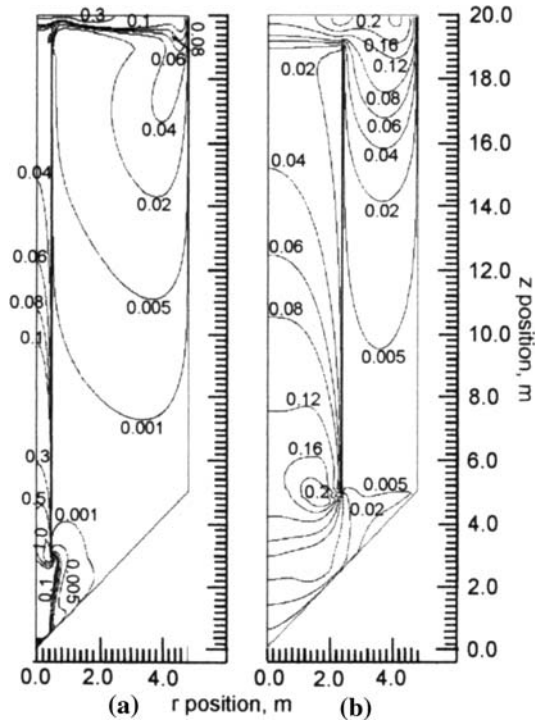


Fig. 18—Predicted distributions of turbulent kinetic energy in industrial-scale Pachuca tanks with (a) $d_d/d_t = 0.1$ and (b) $d_d/d_t = 0.5$. The other conditions are: $u_{sg} = 0.001$ m/s, $d_t = 9.6$ m, $s_d = 0.94$ m, $s_{db} = 2.39$ m, and $h_t/d_t = 2.08$.

ACKNOWLEDGMENTS

The authors gratefully acknowledge research funding from the National Council for Science and Technology of Mexico through Research Grant No. 4407-A9406. One of the authors (ERM) thanks CONACYT for receipt of a postdoctoral scholarship. The authors appreciate the assistance of E.N. Aguilera G. and D.A. Salinas G. with the laboratory work.

NOMENCLATURE

A_a, A_d	cross-sectional area of the annulus; cross-sectional area of draft tube
A_{ct}, A_{cb}	area of the cylindrical surface of height s_d on top of the draft tube; area of the cylindrical surface of height s_{db} below the base of the draft tube, m^2
B_1, B_2	cyclic r - z planes separated by 360 deg
C	concentration of solute tracer, $kg\ m^{-3}$
C_1, C_2, C_d	constants in the turbulence model
d_d, d_t, d_{db}	draft tube diameter; tank tube diameter; thickness of annular section at draft tube base
d_{at}	thickness of annular section at draft tube top, m
D_{eff}	effective diffusion coefficient, $m^2\ s^{-1}$
g	acceleration due to gravity, ms^{-2}

G	rate of generation of k per unit volume, $\text{kg m}^{-1} \text{s}^{-3}$
h_d	height of draft tube, m
h_t, h_d	depth of water bath; height of draft tube, m
I_s	intensity of segregation
k	turbulence kinetic energy, $\text{m}^2 \text{s}^{-2}$
p	pressure, $\text{kg m}^{-1} \text{s}^{-2}$
Q_g, Q_t	volumetric gas flow rate at orifice conditions; circulation liquid flow rate, $\text{m}^3 \text{s}^{-1}$
r, r_d, r_t	radial coordinate; radius of draft tube; radius of tank, m
$E_{\phi P}$	residual of the discretized equation for the flow variable ϕ at node P
s_d, s_{db}	draft tube submergence; draft tube to base separation, m
S_{ϕ}	source term of flow variable ϕ
t	time, s
t_w	draft tube wall thickness, m
u	mean axial velocity component, ms^{-1}
U_{slip}	terminal rising velocity of a single bubble, m/s
$u_{sg}, u_{sg,d}$	superficial gas velocity with respect to the tank diameter; with respect to draft tube diameter, superficial
$u_{sl,d}$	liquid velocity in draft tube, ms^{-1}
v	mean radial velocity component, ms^{-1}
V, V_l	volume of discretization cell; volume of cell occupied by liquid, m^3
$V_o, V_{\infty}, V(t)$	initial voltage across the electrode of the conductivity meter corresponding to an initial solute concentration; voltage corresponding to complete tracer dissolution after a sufficiently long time; voltage corresponding to a certain local tracer concentration at time t , V
Y	degree of mixing
z	axial coordinate, m
$\bar{\alpha}, \bar{\alpha}_{\text{vol}}$	cross-sectional area averaged gas volume fraction; volume-averaged gas fraction in draft tube
ε	dissipation rate of turbulence kinetic energy, $\text{m}^2 \text{s}^{-3}$
ϕ	flow variable
∇	gradient operator in terms of r - z coordinates for the continuity, momentum and turbulence equations and in terms of r - θ - z coordinates for the mass solute tracer concentration equation, m^{-1}
∇	divergence operator in terms of r - z coordinates for the continuity, momentum and turbulence equations and in terms of r - θ - z coordinates for the mass solute tracer concentration equation, m^{-1}
$\mu, \mu_{\tau}, \mu_{\text{eff}}$	molecular, turbulent and effective viscosity, $\text{kg m}^{-1} \text{s}^{-1}$
ρ, ρ_l, ρ_g	local density; liquid density; gas density, kg m^{-3}

$\sigma_C, \sigma_{C,t}$	laminar and turbulent Schmidt numbers for concentration
$\sigma_k, \sigma_{\varepsilon}$	Schmidt numbers for k and ε
θ	circumferential coordinate, radians
Γ_{ϕ}	effective exchange coefficient of the quantity ϕ , $\text{kg m}^{-1} \text{s}^{-1}$

REFERENCES

1. N.N. Clark: *Miner. Metall. Process.*, 1984, Nov. pp. 226–32.
2. C.J. Hallet, A.J. Monhemius, D.G.C. Robertson: *Extraction Metallurgy 1981*, I.M.M., London, 1981, pp. 308–20.
3. R. Shekhar and J.W. Evans: *Metall. Trans. B*, 1989, vol. 20B, pp. 781–91.
4. A.G.W. Lamont: *Can. J. Chem. Eng.*, 1958, Aug., pp. 153–60.
5. P. Weiland: *Ger. Chem. Eng.*, 1984, vol. 7, pp. 374–85.
6. G.M. Fraser: *Aus. I.M.M. Perth and Kalgoorlie Branches, Regional Conf. on Gold-Mining, Metallurgy and Geology*, Oct. 1984, pp. 245–56.
7. F.R. Carrillo P., A. Uribe S., and A.H. Castillejos E.: *Miner. Eng.*, 1995, vol. 8, pp. 405–509.
8. M. Zaisha, Y. Shouzhi, and C. Chen: *Proc. 3rd Int. Symp. on Hydrometallurgy, Research Development and Plant Practice*, K. Osseo-Asare and J.D. Miller, eds., AIME, Atlanta, GA, 1983, pp. 789–806.
9. K. Koide, S. Iwamoto, Y. Takasaka, S. Matsuura, E. Takahashi, M. Kimura, and H. Hubota: *J. Chem. Eng. Jpn.*, 1984, vol. 17, pp. 611–18.
10. K. Koide, K. Horibe, H. Kawabata, and S. Ito: *J. Chem. Eng. Jpn.*, 1984, vol. 17, pp. 369–74.
11. G.G. Roy, R. Shekhar, and S.P. Mehrotra: *Metall. Mater. Trans. B.*, 1998, vol. 29B, pp. 339–49.
12. G.G. Roy and R. Shekhar: *Trans. Inst. Min. Metall.*, 1996, vol. 105, pp. C9–C15.
13. D. Gavroy, C. Joly-Vuillemin, G. Cordier, and H. Delmas: *Trans. I. Chem. E.*, 1995, vol. 73, pp. 637–42.
14. G.G. Roy, A. Bera, and J.H. Mankar: *Trans. Inst. Min. Metall., Sect. C*, 2000, vol. 109, pp. 90–96.
15. R. Shekhar: Ph.D. Thesis, University of California, Berkeley, CA, 1988.
16. R. Shekhar and J.W. Evans: *Metall. Trans. B*, 1990, vol. 21B, pp. 191–203.
17. H. Singh and D. Mazumdar: *Metall. Mater. Trans. B*, 1997, vol. 28B, pp. 727–31.
18. J.S. Woo, J. Szekeley, A.H. Castillejos, and J.K. Brimacombe: *Metall. Trans. B*, 1990, vol. 21B, pp. 269–77.
19. T. DebRoy, A.K. Majumdar, and D.B. Spalding: *Appl. Math. Model.*, 1978, vol. 2, pp. 146–50.
20. J.H. Hills: *Chem. Eng. J.*, 1976, vol. 12, pp. 89–99.
21. *VISIFLOWSystem User Manual*, AEA Technology, Oxford, United Kingdom, 1987, pp. 9:2–9:5.
22. E.N. Aguilera G: M.Sc., CINVESTAV, Unidad Saltillo, Mexico, 1994.
23. G.G. Murthy and J.F. Elliott: *ISIJ*, 1992, vol. 32, pp. 190–95.
24. A.H. Castillejos E. and J.K. Brimacombe: *Metall. Trans. B*, 1987, vol. 18B, pp. 659–71.
25. G.F. Hewitt: *Measurement of Two Phase Flow Parameters*, Academic Press Inc, London, 1978, pp. 11–13.
26. R. Clift, J.R. Grace, and M.E. Weber: *Bubbles, Drops and Particles*, Academic Press Inc., NY, 1978, pp. 171–73.
27. N. El-Kaddah and J. Szekeley: *Ironmaking and Steelmaking*, 1981, vol. 8, pp. 269–78.
28. W.P. Jones and B.E. Launder: *Int. J. Heat Mass Transfer*, 1972, vol. 15, pp. 301–14.
29. B.E. Launder and D.B. Spalding: *Comput. Math. Appl. Mech. Eng.*, 1974, vol. 3, pp. 269–89.
30. PHOENICS 2006, D.B. Spalding, CHAM, Bakery House, London.
31. Esperanza Rodríguez M.: Reporte Interno de Doctorado, CINVESTAV, Feb. 2006.